CHEMISTRY OF MATERIALS

Article

pubs.acs.org/cm

Synthesis and Characterization of ReS_2 and $ReSe_2$ Layered Chalcogenide Single Crystals

Bhakti Jariwala,[†] Damien Voiry,[‡] Apoorv Jindal,[†] Bhagyashree A. Chalke,[†] Rudheer Bapat,[†] Arumugam Thamizhavel,[†] Manish Chhowalla,[‡] Mandar Deshmukh,[†] and Arnab Bhattacharya*[,†]

[†]Department of Condensed Matter Physics and Materials Science, Tata Institute of Fundamental Research, Homi Bhabha Road, Colaba, Mumbai 400005, India

[‡]Materials Science and Engineering, Rutgers University, 607 Taylor Road, Piscataway, New Jersey 08854, United States

Supporting Information

ABSTRACT: We report the synthesis of high-quality single crystals of ReS_2 and $ReSe_2$ transition metal dichalcogenides using a modified Bridgman method that avoids the use of a halogen transport agent. Comprehensive structural characterization using X-ray diffraction and electron microscopy confirm a distorted triclinic 1T' structure for both crystals and reveal a lack of Bernal stacking in ReS_2. Photoluminescence (PL) measurements on ReS_2 show a layer-independent bandgap of 1.51 eV, with increased PL intensity from thicker flakes, confirming interlayer coupling to be negligible in this material. For $ReSe_2$, the bandgap is weakly layer-dependent and decreases from 1.31 eV for thin layers to 1.29 eV in thick flakes. Both chalcogenides show feature-rich Raman spectra whose excitation energy dependence was studied. The lower background doping inherent to our crystal growth process results in high field-effect mobility values of 79 and 0.8 $cm^2/(V\,s)$ for ReS_2 and $ReSe_2$, respectively, as extracted from FET structures fabricated from exfoliated flakes. Our work shows ReX_2 chalcogenides to be promising 2D materials candidates, especially for optoelectronic devices, without the requirement of having monolayer thin flakes to achieve a direct bandgap.

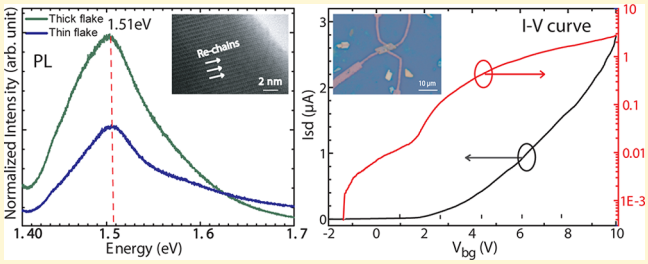

INTRODUCTION

The rhenium-based dichalcogenide materials ReX_2 (X = S and Se) are relatively unexplored members of the class of layered transition metal dichalcogenides (TMDC) that have attracted recent research interest[1−8] because of their unique structural and electronic properties. Most of the well-established TMDCs such as MoS_2 and WS_2 have interesting electronic and optical properties[9] that make them ideally suited for a range of device applications.[10−15] However, these properties are strongly dependent on layer thickness with the best results typically being obtained from monolayers of these 2D materials.[16−18] For example, in monolayer form, MoS_2 has a direct band gap, but the band gap turns indirect with increasing number of layers.[19,20] This puts severe constraints on the versatility of such TMDC materials for optoelectronic device fabrication where a direct bandgap and sufficient active region thickness are important. Recently, ReS_2 was shown to behave as a stack of electronically and vibrationally decoupled monolayers even in bulk form, with its Raman spectrum and photoluminescence properties being independent of the number of layers.[1−3,21] This suggests that ReS_2 could offer a novel system to study mesoscopic physics of 2D systems without the limitation of obtaining large-area, monolayer-thick flakes. Interestingly, another member of the rhenium-based dichalcogenides, $ReSe_2$[4,5,8] is isoelectronic to ReS_2 and could also have unconventional optical and electronic properties. The inherent lattice distortion in $ReSe_2$ makes it a suitable candidate for tuning the magnetic and optical properties via strain engineering.[8] The crystal growth of ReX_2 is, however, a challenge because Re has one of the highest melting points of all metals, whereas S and Se have relatively low melting points and high vapor pressures. Hence, these crystals are typically grown using a halogen vapor transport route using Br_2 or I_2 as a transport agent. This, however, leads to unintentional background doping and changes the electrical properties of the material. Crystals grown by the I_2 vapor transport technique are typically p-type[22,23] while the use of Br_2 usually results in n-type material.[23−28] In this paper we report the growth, under appropriate conditions, of high-quality ReS_2 and $ReSe_2$ single crystals by a modified Bridgman method that does not involve the use of any transport agent. We perform comprehensive structural, optical, and electrical characterization of these crystals and obtain field-effect mobility values of 79 and 0.8 $cm^2/(V\,s)$ for ReS_2 and $ReSe_2$, respectively, significantly higher than previously reported for similar device structures.

SINGLE-CRYSTAL GROWTH

Single crystals of ReS_2 and $ReSe_2$ were grown from the constituent elements directly via a modified Bridgman method

Received: January 29, 2016
Revised: April 24, 2016

DOI: 10.1021/acs.chemmater.6b00364
Chem. Mater. XXXX, XXX, XXX−XXX

by a careful optimization of the growth process using an appropriate temperature profile. The growth was performed in a 2 cm diameter, 20 cm long quartz tube, which was cleaned using HF/H_2O (1:10) solution and rinsed thoroughly with distilled water prior to the growth process. This step is critical because apart from removing impurities the etchant also causes a slight roughening of the inner surface of the tube, which is beneficial in promoting nucleation during the growth. The constituent elements −5N pure Re, and S/Se were weighed in the stoichiometric proportion individually, introduced into the tube and sealed under vacuum (2×10^{-6} mbar). The growth was initiated by placing the ampoule into a vertical Bridgman furnace, with the following temperature profile used to obtain single crystals of the ReX_2 materials. Initially, the temperature was increased to 1100 °C over a 72 h period.[29] Following a stabilization time of 24 h, the temperature was very slowly decreased to 900 °C at the rate of 1 °C/h over a period of 10 days, after which the tube was cooled down to room temperature at the rate of 60 °C/h. This resulted in the formation of shiny crystals in the form of very thin platelike flakes of hundreds of micrometer thickness and approximately 4×5 mm^2 in lateral size. The optical micrographs and SEM images of the grown crystals are shown in Figure S1. For measurement of layer-dependent photoluminescence, Raman spectra, and electrical properties, thin sheets were mechanically exfoliated from these flakes and transferred to SiO_2-coated Si substrates for measurements.

RESULTS AND DISCUSSION

Unlike the common hexagonal (e.g., MoS_2) or octahedral (e.g., WS_2) structures seen in most TMDCs, the rhenium-based dichalcogenides ReS_2 and $ReSe_2$ crystallize in a distorted $1T'$ structure having a triclinic symmetry $P\bar{1}$. Schematic diagrams of the side and top view of such a structure are shown in Figure 1a,b,

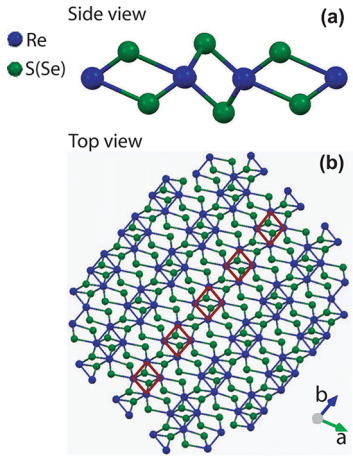

Figure 1. Schematic diagram of atomic arrangement in ReX_2 (X = S and Se): (a) side view and (b) top view along the *c* axis. Here, blue and green circles represent the transition metal and chalcogenide, respectively.

respectively. The d^3 electron configuration in the outermost shell of Re is responsible for the displacement of the metal (Re) atoms from their octahedral position at the center of the anion cage. As a result of the Peierls distortion, the Re atoms dimerize to form diamond-shaped Re chains that extend along the in-plane *b* axis. This results in the ReX_2 materials crystallizing in a stable semiconducting $1T'$ phase with an in-plane anisotropy. The X−Re−X sandwiched layers are stacked along the *c* axis by weak van der Waals forces to form a layered structure. We discuss the detailed characterization of these materials in the sections below.

Structural Analysis. High-resolution X-ray diffraction (HRXRD) measurements were used to evaluate the structural properties of the ReS_2 and $ReSe_2$ single crystals, the data are shown in Figure 2a,b, respectively. An expanded view of the most prominent (0 0 *l*) peak is shown in the inset. For both samples, we observed only the (0 0 *l*) reflections with all other (*hkl*) reflections being absent, suggesting a highly oriented single crystal in the *c* axis direction. The most significant (0 0 1) peak was observed at $2\theta = 14.5$ and 13.5° for ReS_2 (Figure 2a) and $ReSe_2$ (Figure 2b), respectively. The narrow and sharp diffraction peaks, all with <0.1° fwhm values, point to the high crystalline quality of our material, showing that the conventional Bridgman method without utilizing a halogen transport agent can provide high-quality ReX_2 crystals. The crystalline quality of grown crystals were also reaffirmed from diffraction measurements using transmission electron microscopy (TEM) discussed subsequently. The detailed structural parameters such as lattice constants, fwhm, and *d*-spacings extracted from the measured data are presented in Table S1 along with powder diffraction data (Figure S2).

Transmission Electron Microscopy. The detailed atomic arrangement of the ReX_2 crystals was investigated using high-resolution transmission electron microscopy (HRTEM) performed using a 200 kV FEI Tecnai-20 system. Sample preparation details are described in the Methods section. To get information about the in-plane and out-of-plane atomic arrangements, TEM images were obtained for both crystals for two orthogonal viewing axes: parallel to (cross-sectional view) and perpendicular to the basal plane (top view).

Figures 3 and 4 show HRTEM images (a and c) and the corresponding diffraction patterns (b and d) for the ReS_2 and $ReSe_2$ crystals, respectively. Figure 3a shows the cross-sectional TEM image of an ReS_2 sample; the corresponding diffraction pattern along the [−1 2 1] zone axis is shown in Figure 3b, with the simulated pattern shown in the inset. The diffraction patterns were simulated using the JEMS software. The absence of diffraction spots from odd planes of reflection such as (101), (303), and so on indicates a lack of Bernal stacking between the successive layers in ReS_2, which is consistent with the previously reports by Tongay et al.[1] Figure 3c shows the top view of the ReS_2 along the [0 0 1] zone axis, normal to the basal plane, where the Re chains can be clearly seen. The corresponding diffraction pattern and simulation are shown in Figure 3d. It is interesting to note that the intensity of the (2*h*2*k*0) diffraction spots are higher in intensity compared to those from the (*h k* 0) planes, owing to an anisotropic ordering of the Re atoms, with small in-plane displacements from the equilibrium positions.

The HRTEM images and diffraction patterns for $ReSe_2$ are shown in Figure 4. Similar to the case of ReS_2, the cross-sectional view and corresponding diffraction pattern are shown in parts a and b with the top view and the corresponding diffraction pattern are shown in parts c and d. An immediate noticeable point of difference while comparing the diffraction pattern in Figure 4b with that of ReS_2 in Figure 3b is the presence of the diffraction spots from the odd planes of reflection (such (001), (1 −21), etc.) in the $ReSe_2$ case, suggesting that the layers in $ReSe_2$ have a Bernal stacking arrangement, unlike those in ReS_2. As expected, the top view is rather similar, with the familiar Re chains being present and the diffraction pattern pointing to an anisotropic atomic arrangement.

DOI: 10.1021/acs.chemmater.6b00364
Chem. Mater. XXXX, XXX, XXX−XXX

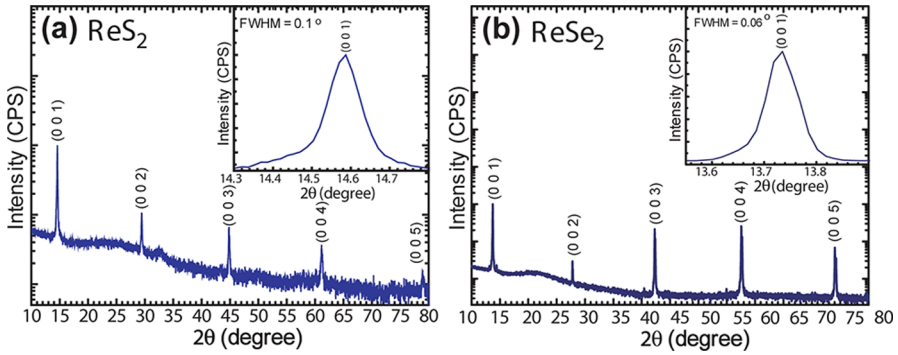

Figure 2. HRXRD 2θ scan for (a) ReS_2 and (b) $ReSe_2$ single crystals. The patterns were indexed with International Centre for Diffraction Data Powder Diffraction Files 00-052-0818 and 04-007-1113, [2014], for ReS_2 and $ReSe_2$, respectively. The *y* axis is plotted on a log scale. Insets show expanded views of the most prominent reflection. The absence of other (*hkl*) reflections and the small fwhm values of 0.1 and 0.06° for (0 0 1) reflection of ReS_2 and $ReSe_2$, respectively, point to the high crystal quality.

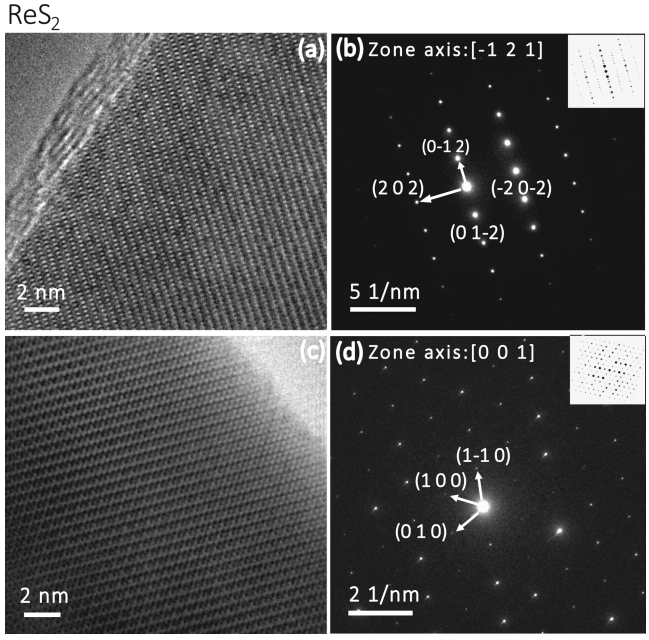

Figure 3. HRTEM images of ReS_2. (a) Cross-sectional view with the electron beam directed parallel to the basal plane; (b) corresponding diffraction pattern centered on the [−1 2 1] zone axis, with the simulate diffraction pattern shown in the inset. Here, the absence of the diffraction spots from the (1 0 1), (3 0 3), ... planes of reflection shows the lack of Bernal stacking in ReS_2. (c) Top view, with the electron beam direction normal to the basal plane; (d) corresponding diffraction pattern centered on the [0 0 1] zone axis, with the simulated diffraction pattern in the inset.

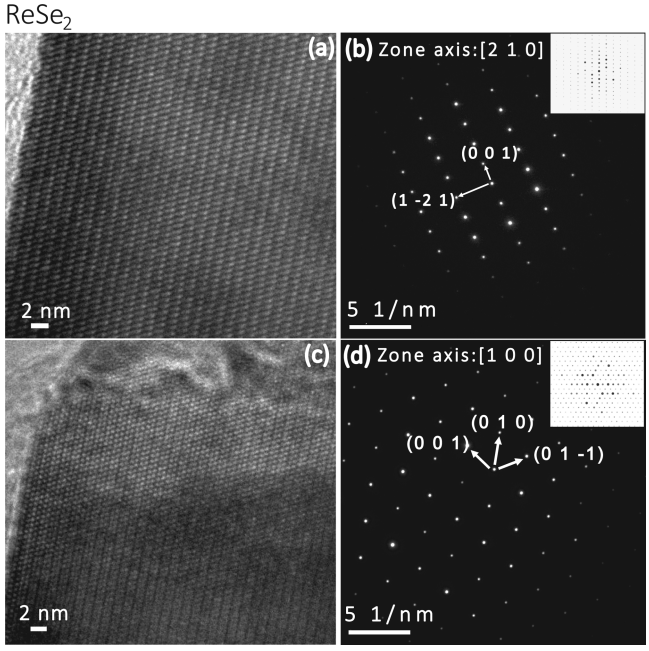

Figure 4. HRTEM images of $ReSe_2$. (a) Cross-sectional view with electron beam directed parallel to the basal plane; (b) corresponding diffraction pattern centered on the [2 1 0] zone axis, with the simulated diffraction pattern shown in the inset. (c) Top view, with the electron beam direction normal to the basal plane; (d) corresponding diffraction pattern centered on the [1 0 0] zone axis, with simulated diffraction pattern shown in the inset.

X-ray Photoelectron Spectroscopy. The compositional and core level elemental analysis of the crystals were characterized by energy dispersive X-ray spectroscopy (EDX) and X-ray photoelectron spectroscopy (XPS). The stoichiometry of the sample was determined from EDX analysis, where the observation of a 1:2 atomic ratio of metal (Re) to chalcogenide (S and Se) (see section 4 in the Supporting Information for details) confimed the formation of the ReX_2 phase. The core level elemental analysis of the valence band energy levels of the Re atom (Figure 5a,c) shows the f shell splitting into the $4f_{7/2}$ and $4f_{5/2}$ sublevels with an energy difference of 2.4 eV, consistent with the expected Re metal peak splitting. However, the peak positions of the $4f_{7/2}$ and $4f_{5/2}$ features at 42.18 and 44.58 eV for both ReS_2 and $ReSe_2$, respectively, indicate a blueshift by 1.68 eV in comparison to the standard position[30] of the 4f core level peaks of metallic Re at 40.5 and 42.9 eV. Such energy shifts of the 4f levels could be due to the bonding of chalcogens atoms to rhenium in the ReX_2. In the case of chalcogens, the 2p core level peaks, $2p_{3/2}$ and $2p_{1/2}$ of S atom and 3d core level peaks, $3d_{5/2}$ and $3d_{3/2}$ of Se atoms are located at 161.58 and 167.28 eV and 55.48 and 56.28 eV, respectively, consistent with the reported work on bulk ReS_2.[31] The details of the peak positions and corresponding line widths are listed in Table S6.

Raman Spectroscopy. The atomic vibrational spectra of layers exfoliated from the ReS_2 and $ReSe_2$ crystals were recorded using three different laser excitation wavelengths, 514, 532, and 633 nm to understand the wavelength-dependent behavior of the Raman modes. The exfoliation was carried out mechanically using Scotch tape with the layers being transferred to silicon

DOI: 10.1021/acs.chemmater.6b00364
Chem. Mater. XXXX, XXX, XXX−XXX

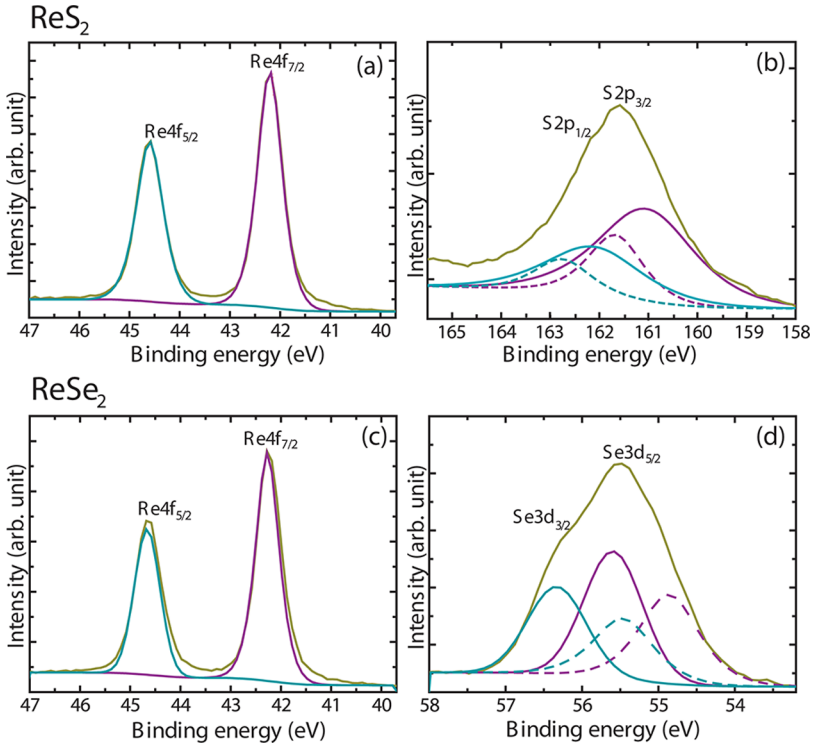

Figure 5. XPS spectra of the ReS_2 and $ReSe_2$ crystals. Core level 4f shell peaks $4f_{7/2}$ and $4f_{5/2}$ of the Re atom for (a) ReS_2 and (c) $ReSe_2$. The chalcogens' outer shells are $2p_{3/2}$ and $2p_{1/2}$ core levels for the (b) S 2p feature and $3d_{5/2}$ and $3d_{3/2}$ core levels for the (d) Se 3d feature.

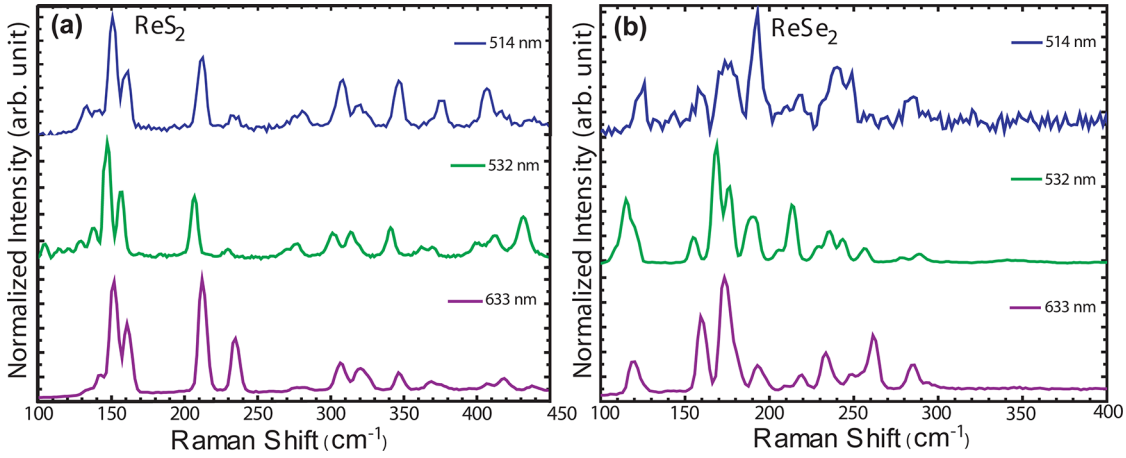

Figure 6. Normalized Raman scattering spectra measured at 514, 532, and 633 nm excitation energy for exfoliated (a) ReS_2 and (b) $ReSe_2$ on a SiO_2/Si substrate. The thickness of the flake was ~2 nm.

substrates coated with a 300 nm thick thermal oxide layer on top of it. All the measurements were recorded at room temperature. The laser power was kept at 0.5 μW to avoid heating the samples. The Raman spectra of 2 nm thick flakes of ReS_2 and $ReSe_2$, excited at different laser wavelengths, are shown in Figure 6a,b. Unlike other members of TMDCs such as MoX_2 and WX_2, the Raman spectra of the Re based dichalcogenides are feature-rich with about 18 first-order Raman active modes in the range of 100−300 cm^{-1}, which are nondegenerate because of their low symmetry structure. Interestingly, they exhibit novel vibrational properties such as the absence of active in-plane vibrational modes $E_{2g}{}^1$ and $E_{2g}{}^2$ (Figure 6) mode below ≤100 cm^{-1} due to the presence of only one layer in their unit cell rather than two in MoS_2 or three in WS_2 unit cell, respectively. All expected active in-plane and out-of plane vibrational modes along with the contracted mode of Re, S, and Se are observed. Two intense and characteristic vibration modes are observed at 150 and 212 cm^{-1} for ReS_2 and 124 and 158 cm^{-1} in the case of $ReSe_2$, which is consistent with the literature.[1−4,32] The observed in-plane and out of plane vibrations are in reasonable agreement with the recent simulated and experimental values reported by Feng et al.[3] The in-plane vibrational modes appear at 156, 168.4, 212.2, and 236.8 cm^{-1} for Re atoms and 308.2 and 313.5 cm^{-1} in the case of S atoms. The same matching was observed for out-of plane vibrations located at 133.1 and 141.9 cm^{-1} for Re and 421.7 and 445.8 cm^{-1} for S atoms, along with the contracted vibrations of Re−S atoms, 275.1 and 280.4 cm^{-1}. Apart from the difference in the outermost electron configuration, $ReSe_2$ belongs to the same structure formation as ReS_2 and as expected shows nearly the same number of active vibrational modes in its Raman spectrum,

DOI: 10.1021/acs.chemmater.6b00364
Chem. Mater. XXXX, XXX, XXX−XXX

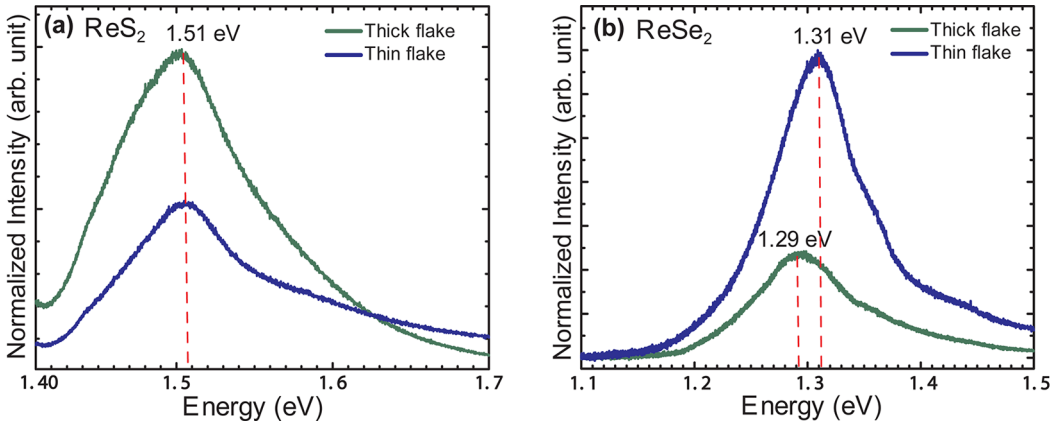

Figure 7. Room-temperature PL spectra of thin (~2 nm) and thick (~10 nm) flakes of (a) ReS_2 and (b) $ReSe_2$. The flakes were exfoliated onto a SiO_2/Si substrate and a 633 nm laser was used for excitation.

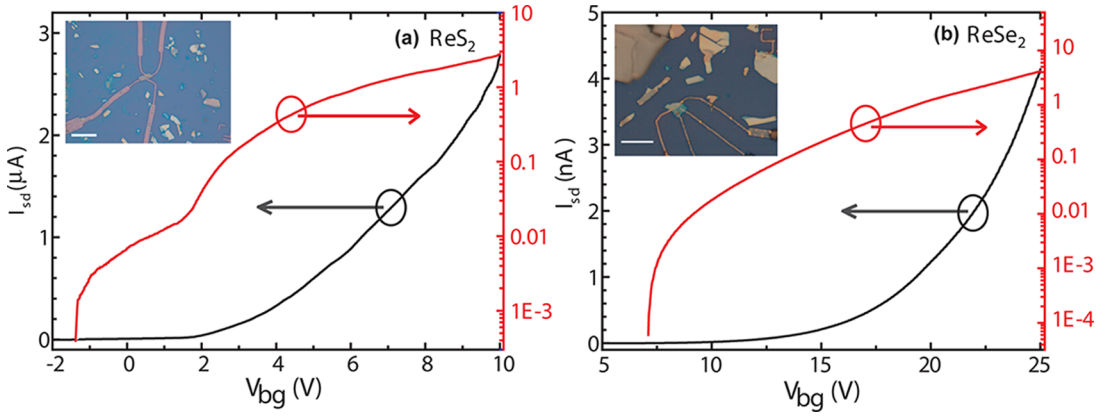

Figure 8. Electrical characterization (I_{ds}–V_{bg}) of FET structures. Room-temperature transfer characteristics at V_{ds} = 200 mV for (a) ReS_2 and (b) $ReSe_2$. The insets show optical images of the devices; the scale bar is 10 μm in both images. The two steps in the curve for ReS_2 arise from the flake having regions of two different thicknesses. See Supporting Information for an enlarged view of the device.

as seen in Figure 6b. Comparative Raman spectra for layers of different thickness are shown in Supporting Information section 5.

Photoluminescence Measurements. The dependence of photoluminescence (PL) properties with sample thickness provides a simple way to verify the weak interlayer coupling in the 1T' stucture and check for a crossover from direct to indirect band gap. Figure 7a shows the room-temperature PL spectra from exfoliated ReS_2 flakes of two different thickness denoted as the thin (~2 nm) and thick (~10 nm) samples. The PL peaks were observed at the same energy position, 1.51 eV, for both thin and thick flakes, consistent with the previously reported values for the bulk.[1] Furthermore, the peak intensity is higher for the thicker layer than thinner one, as was also reported in refs 1 and 7. This is in sharp contrast to the typical behavior seen in Mo- and W-based TMDCs and confirms that ReS_2 behaves as a stack of decoupled monolayers even in bulk form. In the case of $ReSe_2$, the corresponding PL spectra for thick and thin samples are shown in Figure 7b. The peak position shifts slightly from 1.31 eV for the thin layer to 1.29 eV for the thick layer. This is similar to the report by Zhao et al.[33] (~1.27 eV for 10L and ~1.32 eV for 2L) and also agrees with the observations of Yang et al.[8] (~1.44 eV for a monolayer flake, with much of the blueshift with reducing thickness occurring close to the one ML limit).

Furthermore, the intensity of the luminescence is also weaker for the thicker layer. However, the drop in luminescence with thickness is not as drastic as that for the Mo- and W-based TMDCs, suggesting that there is a very weak but non-negligible interlayer coupling. Unlike MoS_2, the presence of structural distortion results in a lesser charge difference between the Re layer and chalcogens (S and Se) layers leading to a weaker interlayer interaction in ReX_2. These observations are consistent with the structural information evaluated from XRD and electron microscopy reported in the earlier sections where the presence of structural distortion is lesser in $ReSe_2$ compared to ReS_2.

Electrical Measurements. Electrical properties of the ReS_2 and $ReSe_2$ crystals were evaluated by characterizing thin-film field-effect transistors (FET) fabricated on mechanically exfoliated flakes transferred to a 300 nm SiO_2-coated p^{++} Si wafer. Thin flakes were identified by optical contrast and AFM. FETs were fabricated with these flakes as channel using standard lithography techniques. Source and drain contacts were defined by thermal evaporation of 10/70 nm Cr/Au followed by lift-off in acetone. The transfer characteristics for ReS_2 and $ReSe_2$ devices are shown in Figure 8a,b, respectively, with optical images of the fabricated devices shown in the insets. I_{ds}–V_{ds} curves are provided in the Supporting Information. On performing electrostatic gating, ReS_2 and $ReSe_2$ are both observed to be n-type. For $ReSe_2$, this behavior is contrary to previous reports.[5] We attribute this to the absence of a transport agent, such as I_2, during the growth process, which can cause charge compensation. We extract field-effect mobility from the linear part of the

DOI: 10.1021/acs.chemmater.6b00364
Chem. Mater. XXXX, XXX, XXX–XXX

Table 1. Comparison of Electrical Data Reported for ReS_2 and $ReSe_2$ Field-Effect Transistor Structures

refs	mobility (no. of layers) ($cm^2/(Vs)$)	I_{on}/I_{off} ratio	channel dimension (μm)	V_{ds} (V)
n-ReS_2 (our data)	79.1 (28L)	750	L, 0.7; W, 2.1	200 mV
n-ReS_2 [32]	0.072 (1L)	10^3	L, 2; W, 5	
n-ReS_2 [34]	0.1−2.6 (1L)	10^7		100 mV
	15.4 (6L)	10^7 (7L)		
n-ReS_2 [35]	23.1 (1L) (∥-*b* axis)	10^6	L, 0.7; W, 0.3	−3 V
	14.8 (1L) (⊥-*b* axis)			
	4.7 (few layer)			
n-ReS_2 [36]	30 (11L)	10^4−10^5	L, 16; W, 1.6	150 mV
n-ReS_2 [37]	5−30 (3−6 layers)	10^8		1 V
n-$ReSe_2$ (our data)	0.8 (35L)	10^4	L, 6.4; W, 2.5	200 mV
p-$ReSe_2$ [5]	9.78 (1L)		L, 2; W, 2	−1 V
	0.10 (4L)			

gating curve using the formula $\mu_{FE} = (dI_{ds}/dV_g) \times (L/W) \times (1/(\epsilon_{ox}V_{bias}))$, where ϵ_{ox} is the capacitance per unit area between channel and back gate. For our case, $\epsilon_{ox} = 1.15 \times 10^{-4}$ F/m^2. The mobility for ReS_2 is calculated to be 79.1 $cm^2/(Vs)$, whereas for $ReSe_2$, it is 0.8 $cm^2/(Vs)$. The mobility values for the two materials are significantly higher than those previously reported values for multilayered ReS_2 (15.4 $cm^2/(V\,s)$)[34] and $ReSe_2$ (0.10 $cm^2/(V\,s)$)[5] FETs, again reflecting the improved crystal quality. A summary of mobility values obtained by various groups is presented in Table 1. We report an I_{on}/I_{off} of 2.7×10^3 for ReS_2 and 3.0×10^4 for $ReSe_2$. The transconductance of the device is observed to be 780 and 0.11 nS/μm for ReS_2 and $ReSe_2$, respectively.

CONCLUSIONS

Using a modified Bridgman method, we have successfully grown high-quality single crystals of ReS_2 and $ReSe_2$ without the use of a halogen transport agent. The crystals were comprehensively characterized using HRXRD and TEM, which revealed a distorted triclinic 1T' structure for both crystals. However, the lack of Bernal stacking in ReS_2 was confirmed from the HRTEM. Both chalcogenides show rich Raman spectra whose excitation energy dependence was studied. Photoluminescence measurements revealed a layer-independent bandgap value of 1.51 eV for ReS_2, with increased PL intensity for thicker flakes, thus confirming the absence of interlayer coupling in this material. For $ReSe_2$, the bandgap decreased from 1.31 eV for thin layers to 1.29 eV in thick flakes, suggesting a non-neglible interlayer interaction, which is however weaker than that of the usual Mo- and W-based TMDCs. Electrical measurements on FETs fabricated show a remarkably improved field-effect mobility because of the lower background doping. Our studies confirm the recently observed atypical properties of these materials and show the ReX_2 series to be useful candidates for optoelectronic TMDC devices without the necessity to achieve monolayer thin flakes of the materials.

METHODS

Mechanical Exfoliation of ReX_2. Few-layer ReX_2 nanosheets were exfoliated mechanically using Scotch tape from bulk ReS_2 and $ReSe_2$ single crystals individually and transferred to doped-Si substrates covered with thermally deposited oxide of 300 nm thickness.

XRD, EDX, and XPS Analysis. The high-resolution X-ray diffraction and the powder X-ray diffraction were measured using Panalytical X'Pert Pro system for single crystal and powder samples, respectively, using a Cu Kα source and a step size of 0.016°. The EDX measurement was done using an Oxford Inca Energy EDS. The core level elemental analysis of the present elements was carried out using an X-ray photoelectron spectroscope (AXIS ULTRA-DLD, Shimadzu) with Al Kα source using an X-ray monochromator.

Electron Microscopy. The surface morphology of the as-grown crystals was observed by scanning electron microscopy using a Zeiss Ultra FESEM at an accelerating voltage of 5 kV. Transmission electron microscopy (TEM) was carried out using a FEI Tecnai 20 at an operating voltage of 200 kV (filament: LaB_6). For sample preparation for in-plane view, bulk flakes were stuck face-to-face using G1 epoxy and cured at 130 °C for 15 min. This sandwich material was placed in a slotted Ti grid and again cured at 130 °C for 5 min. The sample was next thinned down to 80−100 μm by polishing from both sides of the disc. After making a dimple of around 20 μm, sample was ion-milled at 3 kV until a hole appeared at the center. As a final step, it was polished at 0.5 kV until the region around the hole became thin enough to be electron transparent.

Raman and PL Measurements. To understand the layer-dependent atomic vibrational properties of the ReX_2 samples, the Raman measurement was carried out on different thickness flakes, thin flake (∼2 nm) and thick flake (∼10 nm), at three different laser excitation wavelengths (Figure S6). The Raman signals at 514 and 633 nm wavelengths were measured using a Renishaw PL/Raman system, whereas the 532 nm wavelength measurement was recorded using a Witec alpha 300R confocal Raman microscope. The variation of the bandgap with the number of layers was also checked using PL spectroscopy. The luminescence was measured at three different excitation wavelengths, 514, 532, and 633 nm, for both ReS_2 and $ReSe_2$. All the measurements were carried out at room temperature.

Device Fabrication. FET devices were demonstrated on mechanically exfoliated flakes transferred to 300 nm SiO_2-coated heavily doped silicon wafers using the Scotch tape technique. Thin flakes were identified by optical contrast and AFM. FETs were fabricated with these flakes as channel using standard electron beam lithography techniques. Contacts of Cr/Au (10 nm/70 nm) were realized by thermal evaporation at ∼5 Å/s followed by liftoff in acetone. All electrical measurements were performed on wire-bonded samples in a homemade measurement setup under vacuum condition ($\leq 10^{-5}$ mbar) at room temperature in dark.

ASSOCIATED CONTENT

Supporting Information

The Supporting Information is available free of charge on the ACS Publications website at DOI: 10.1021/acs.chemmater.6b00364.

Optical and SEM images of crystals; powder XRD profiles and analysis; additional TEM images; compositional analysis using EDX and XPS; and additional Raman, PL, and electrical measurements. (PDF)

DOI: 10.1021/acs.chemmater.6b00364
Chem. Mater. XXXX, XXX, XXX−XXX

AUTHOR INFORMATION

Corresponding Author

*E-mail: arnab@tifr.res.in. Phone: +91-22-22782517. Fax: +91-22-22804610.

Notes

The authors declare no competing financial interest.

ACKNOWLEDGMENTS

We thank D. V. Savant for help with ampoule preparation and vacuum sealing and N. Hatui for HRXRD measurements. The work at TIFR was supported through internal grants 12P0168 and 12P0169.

REFERENCES

(1) Tongay, S.; Sahin, H.; Ko, C.; Luce, A.; Fan, W.; Liu, K.; Zhou, J.; Huang, Y. S.; Ho, C. H.; Yan, J.; Ogletree, D. F. Monolayer Behaviour in Bulk ReS_2 due to Electronic and Vibrational Decoupling. *Nat. Commun.* **2014**, *5*, 3252.

(2) Chenet, D. A.; Aslan, O. B.; Huang, P. Y.; Fan, C.; van der Zande, A. M.; Heinz, T. F.; Hone, J. C. In-Plane Anisotropy in Mono-and Few-Layer ReS_2 Probed by Raman Spectroscopy and Scanning Transmission Electron Microscopy. *Nano Lett.* **2015**, *15*, 5667−5672.

(3) Feng, Y.; Zhou, W.; Wang, Y.; Zhou, J.; Liu, E.; Fu, Y.; Ni, Z.; Wu, X.; Yuan, H.; Miao, F.; Wang, B.; et al. Raman Vibrational Spectra of Bulk to Monolayer ReS_2 with Lower Symmetry. *Phys. Rev. B: Condens. Matter Mater. Phys.* **2015**, *92*, 054110.

(4) Wolverson, D.; Crampin, S.; Kazemi, A. S.; Ilie, A.; Bending, S. J. Raman Spectra of Monolayer, Few-layer, and Bulk $ReSe_2$: An Anisotropic Layered Semiconductor. *ACS Nano* **2014**, *8*, 11154−11164.

(5) Yang, S.; Tongay, S.; Li, Y.; Yue, Q.; Xia, J. B.; Li, S. S.; Li, J.; Wei, S. H. Layer-Dependent Electrical and Optoelectronic Responses of $ReSe_2$ Nanosheet Transistors. *Nanoscale* **2014**, *6*, 7226−7231.

(6) Zhang, E.; Jin, Y.; Yuan, X.; Wang, W.; Zhang, C.; Tang, L.; Liu, S.; Zhou, P.; Hu, W.; Xiu, F. ReS_2-Based Field-Effect Transistors and Photodetectors. *Adv. Funct. Mater.* **2015**, *25*, 4076−4082.

(7) Aslan, O. B.; Chenet, D. A.; van der Zande, A. M.; Hone, J. C.; Heinz, T. F. Linearly Polarized Excitons in Single- and Few-Layer ReS_2 Crystals. *ACS Photonics* **2016**, *3*, 96−101.

(8) Yang, S.; Wang, C.; Sahin, H.; Chen, H.; Li, Y.; Li, S. S.; Suslu, A.; Peeters, F. M.; Liu, Q.; Li, J.; Tongay, S. Tuning the Optical, Magnetic, and Electrical Properties of $ReSe_2$ by Nanoscale Strain Engineering. *Nano Lett.* **2015**, *15*, 1660−1666.

(9) Li, H.; Zhang, Q.; Yap, C. C. R.; Tay, B. K.; Edwin, T. H. T.; Olivier, A.; Baillargeat, D. From Bulk to Monolayer MoS_2: Evolution of Raman Scattering. *Adv. Funct. Mater.* **2012**, *22*, 1385−1390.

(10) Perea-Lopez, N.; Elias, A. L.; Berkdemir, A.; Castro Beltran, A.; Gutierrez, H. R.; Feng, S.; Lv, R.; Hayashi, T.; Lopez-Urias, F.; Ghosh, S.; Muchharla, B.; et al. Photosensor Device Based on Few-Layered WS_2 Films. *Adv. Funct. Mater.* **2013**, *23*, 5511−5517.

(11) Voiry, D.; Yamaguchi, H.; Li, J.; Silva, R.; Alves, D. C.; Fujita, T.; Chen, M.; Asefa, T.; Shenoy, V. B.; Eda, G.; Chhowalla, M. Enhanced Catalytic Activity in Strained Chemically Exfoliated WS_2 Nanosheets for Hydrogen Evolution. *Nat. Mater.* **2013**, *12*, 850−855.

(12) Huo, N.; Kang, J.; Wei, Z.; Li, S. S.; Li, J.; Wei, S. H. Novel and Enhanced Optoelectronic Performances of Multilayer MoS_2-WS_2 Heterostructure Transistors. *Adv. Funct. Mater.* **2014**, *24*, 7025−7031.

(13) Jo, S.; Ubrig, N.; Berger, H.; Kuzmenko, A. B.; Morpurgo, A. F. Mono-and Bilayer WS_2 Light-Emitting Transistors. *Nano Lett.* **2014**, *14*, 2019−2025.

(14) Perea-Lopez, N.; Lin, Z.; Pradhan, N. R.; Iniguez-Rabago, A.; Elías, A. L.; McCreary, A.; Lou, J.; Ajayan, P. M.; Terrones, H.; Balicas, L.; Terrones, M. CVD-Grown Monolayered MoS_2 as an Effective Photosensor Operating at Low-Voltage. *2D Mater.* **2014**, *1*, 011004.

(15) Mao, D.; Wang, Y.; Ma, C.; Han, L.; Jiang, B.; Gan, X.; Hua, S.; Zhang, W.; Mei, T.; Zhao, J. WS_2 Mode-Locked Ultrafast Fiber Laser. *Sci. Rep.* **2015**, *5*, 7965.

(16) Zhao, W.; Ghorannevis, Z.; Chu, L.; Toh, M.; Kloc, C.; Tan, P. H.; Eda, G. Evolution of Electronic Structure in Atomically Thin Sheets of WS_2 and WSe_2. *ACS Nano* **2013**, *7*, 791−797.

(17) Gutierrez, H. R.; Perea-Lopez, N.; Elias, A. L.; Berkdemir, A.; Wang, B.; Lv, R.; Lopez-Urias, F.; Crespi, V. H.; Terrones, H.; Terrones, M. Extraordinary Room-temperature Photoluminescence in Triangular WS_2 Monolayers. *Nano Lett.* **2013**, *13*, 3447−3454.

(18) Gong, Y.; Lin, J.; Wang, X.; Shi, G.; Lei, S.; Lin, Z.; Zou, X.; Ye, G.; Vajtai, R.; Yakobson, B. I.; et al. Vertical and In-plane Heterostructures from WS_2/MoS_2 Monolayers. *Nat. Mater.* **2014**, *13*, 1135−1142.

(19) Mak, K. F.; Lee, C.; Hone, J.; Shan, J.; Heinz, T. F. Atomically Thin MoS_2: a New Direct-gap Semiconductor. *Phys. Rev. Lett.* **2010**, *105*, 136805.

(20) Splendiani, A.; Sun, L.; Zhang, Y.; Li, T.; Kim, J.; Chim, C. Y.; Galli, G.; Wang, F. Emerging Photoluminescence in Monolayer MoS_2. *Nano Lett.* **2010**, *10*, 1271−1275.

(21) Yu, Z. G.; Cai, Y.; Zhang, Y. W. Robust Direct Bandgap Characteristics of One-and Two-Dimensional ReS_2. *Sci. Rep.* **2015**, *5*, 13783.

(22) Wheeler, B. L.; Leland, J. K.; Bard, A. J. Semiconductor Electrodes. *J. Electrochem. Soc.* **1986**, *133*, 358−361.

(23) Leicht, G.; Berger, H.; Levy, F. The Growth of n-and p-type ReS_2 and $ReSe_2$ Single Crystals and their Electrical Properties. *Solid State Commun.* **1987**, *61*, 531−534.

(24) Marzik, J. V.; Kershaw, R.; Dwight, K.; Wold, A. Photoelectronic Properties of ReS_2 and $ReSe_2$ Single Crystals. *J. Solid State Chem.* **1984**, *51*, 170−175.

(25) Ho, C. H.; Huang, Y. S.; Tiong, K. K. In-plane Anisotropy of the Optical and Electrical Properties of ReS_2 and $ReSe_2$ Layered Crystals. *J. Alloys Compd.* **2001**, *317-318*, 222−226.

(26) Ho, C. H.; Yen, P. C.; Huang, Y. S.; Tiong, K. K. Photoreflectance Study of the Excitonic Transitions of Rhenium Disulphide Layer Compounds. *Phys. Rev. B: Condens. Matter Mater. Phys.* **2002**, *66*, 245207.

(27) Tiong, K. K.; Ho, C. H.; Huang, Y. S. The Electrical Transport Properties of ReS_2 and $ReSe_2$ Layered Crystals. *Solid State Commun.* **1999**, *111*, 635−640.

(28) Friemelt, K.; Akari, S.; Lux Steiner, M. C.; Schill, T.; Bucher, E.; Dransfeld, K. Scanning Tunneling Microscopy with Atomic Resolution on ReS_2 Single Crystals Grown by Vapor Phase Transport. *Ann. Phys.* **1992**, *504*, 248−253.

(29) Because the phase diagrams for Re−S and Re−Se and melting point data are not available in the literature or in standard materials databases, we chose a temperature similar to that used for the tungsten chalcogenides.

(30) Wagner, C. D.; Muilenberg, G. E. *Handbook of X-ray Photoelectron Spectroscopy: A Reference Book of Standard Data for Use in X-ray Photoelectron Spectroscopy*; Physical Electronics Division, Perkin-Elmer Corp.: Eden Prairie, MN, 1979.

(31) Fujita, T.; Ito, Y.; Tan, Y.; Yamaguchi, H.; Hojo, D.; Hirata, A.; Voiry, D.; Chhowalla, M.; Chen, M. Chemically Exfoliated ReS_2 nanosheets. *Nanoscale* **2014**, *6*, 12458−12462.

(32) Keyshar, K.; Gong, Y.; Ye, G.; Brunetto, G.; Zhou, W.; Cole, D. P.; Hackenberg, K.; He, Y.; Machado, L.; Kabbani, M.; Hart, A. H.; et al. Chemical Vapor Deposition of Monolayer Rhenium Disulfide (ReS_2). *Adv. Mater.* **2015**, *27*, 4640−4648.

(33) Zhao, H.; Wu, J.; Zhong, H.; Guo, Q.; Wang, X.; Xia, F.; Yang, L.; Tan, P.; Wang, H. Interlayer Interactions in Anisotropic Atomically Thin Rhenium Diselenide. *Nano Res.* **2015**, *8*, 3651−3661.

(34) Liu, E.; Fu, Y.; Wang, Y.; Feng, Y.; Liu, H.; Wan, X.; Zhou, W.; Wang, B.; Shao, L.; Ho, C. H.; Huang, Y. S. Integrated Digital Inverters based on Two-dimensional Anisotropic ReS_2 Field-effect Transistors. *Nat. Commun.* **2015**, *6*, 6991.

(35) Lin, Y. C.; Komsa, H. P.; Yeh, C. H.; Bjorkman, T.; Liang, Z. Y.; Ho, C. H.; Huang, Y. S.; Chiu, P. W.; Krasheninnikov, A. V.; Suenaga, K. Single-Layer ReS_2: Two-Dimensional Semiconductor with Tunable In-Plane Anisotropy. *ACS Nano* **2015**, *9*, 11249−11257.

(36) Pradhan, N. R.; McCreary, A.; Rhodes, D.; Lu, Z.; Feng, S.; Manousakis, E.; Smirnov, D.; Namburu, R.; Dubey, M.; Hight Walker,

DOI: 10.1021/acs.chemmater.6b00364
Chem. Mater. XXXX, XXX, XXX−XXX

A. R.; Terrones, H.; et al. Metal to Insulator Quantum-phase Transition in Few-layered ReS_2. *Nano Lett.* **2015**, *15*, 8377−8384.
(37) Liu, E.; Long, M.; Zeng, J.; Luo, W.; Wang, Y.; Pan, Y.; Zhou, W.; Wang, B.; Hu, W.; Ni, Z.; You, Y.; et al. High Responsivity Phototransistors based on Few-layer ReS_2 for Weak Signal Detection. *Adv. Funct. Mater.* **2016**, *26*, 1938−1944.

DOI: 10.1021/acs.chemmater.6b00364
Chem. Mater. XXXX, XXX, XXX−XXX